Characterization of Mixing in a Simple Paddle Mixer Using Experimentally Derived Velocity Fields

Douglas Bohl[1], Naratip Santitissadeekorn[2], Akshey Mehta[1], and Erik Bollt[2]
[1]Department of Mechanical and Aeronautical Engineering
[2]Department of Mathematics
Clarkson University
Potsdam, NY

Abstract

The flow field in a cylindrical container driven by a flat bladed impeller was investigated using Particle Image Velocimetry (PIV). Three Reynolds numbers (0.02, 8, 108) were investigated for different impeller locations within the cylinder. The results showed that vortices were formed at the tips of the blades and rotated with the blades. As the blades were placed closer to the wall the vortices interacted with the induced boundary layer on the wall to enhance both regions of vorticity. Finite Time Lyapunov Exponents (FTLE) were used to determine the Lagrangian Coherent Structure (LCS) fields for the flow. These structures highlighted the regions where mixing occurred as well as barriers to fluid transport. Mixing was estimated using zero mass particles convected by numeric integration of the experimentally derived velocity fields. The mixing data confirmed the location of high mixing regions and barriers shown by the LCS analysis. The results indicated that mixing was enhanced within the region described by the blade motion as the blade was positioned closed to the cylinder wall. The mixing average within the entire tank was found to be largely independent of the blade location and flow Reynolds number.

I. Introduction

I.1 Background

Mixing is a fundamental process in many natural and industrial flow fields. In flows such as the current one under investigation (i.e. highly viscous, low speed flows),

small-scale motions are not available and mixing is a result of large-scale motion in the flow. Batch mixers, similar to food mixers, are a primary method for the processing of many materials. However, there are inherent drawbacks to a batch mixing process (e.g. inconsistent mixture quality, residual voids and fissures, limited pot life, etc.).

The study of these devices is complicated by several factors which include rheological properties of the fluids, complex geometries, and device scaling issues. Recent interest in developing more efficient, controllable mixing processes has focused attention on developing a better understanding on the physics of these devices.

The development of computational tools is attractive in that computational tools allow for relatively rapid and simple changes to both geometry and operating conditions to determine optimal mixing protocols. Many researchers have investigated batch mixing configurations numerically (e.g. [1-4]). Stretching and mixing has been a primary interest [1, 2, 4] while fluid properties and power consumption[3] have also been a focus. Computational models have also been utilized to study other mixer configurations (e.g. continuous mixers [5-7], static mixers [8, 9]).

Experimental work on planetary mixers has historically centered on scalar measurements such as power consumption, mixing patterns or final mixture characterization. Zhou et al. [10] investigated the power consumption in a double planetary mixer with Newtonian and non-Newtonian fluids. It was found that the power curve for non-Newtonian fluids was found to collapse to the curve for Newtonian fluids when the Metzner-Otto Reynolds number was used for scaling. Clifford et al. [11] studied the effects of Reynolds number on the mixing in a simplified pin planetary mixer. Mixing patterns were derived using flow visualization and compared to computed fields.

The mixing patterns were found to have a Reynolds number dependence. At low Reynolds number, simulating Stokes flow, the mixing occurred in local regions of the tank limited by the motion of the pin. As the Reynolds number was increased the mixing was observed over progressively larger regions in the tank.

Youcefi et al. [12] experimentally and computationally investigated the effect of fluid elasticity on the flow induced by a rotating flat plate impeller. In this work torque measurements were also made and used to determine the power number as a function of the fluid type and Reynolds number. It was found that the power number data collapsed onto a single curve for all Newtonian and non-Newtonian pseudoplastic fluids when the effective Reynolds number was used for the pseudoplastic fluids.

Recently researchers have started to apply optical measurement techniques to better understand the flow fields in many different mixing devices. Bohl [13] utilized Particle Image Velocimetry (PIV) velocity data to investigate the flow in a simplified batch mixer. Jaffer et al. [14] applied PIV to kneading elements in a twin-screw extruder. Bakalis and Karwe [15] used Laser Doppler Velocimetry (LDV) to measure the velocity profiles in the nip and translation regions of a twin-screw extruder. Yoon et al. [16] investigated the flow in a Rushton turbine using PIV. Utomo et al. [17] combined LDV and computational simulations to quantify the flow patterns and energy dissipation in a batch rotor-stator mixer. These studies have shown the utility in applying non-intrusive diagnostic technique to better understand the flow fields in these devices.

I.2 Dynamical Systems Approach – Lagrangian Coherent Structures

The study of Lagrangian Coherent Structures (LCS) was introduced by Haller as a mathematical formalism based on Finite Time Lyapunov Exponents (FTLE) [18-22]. The

LCS's are descriptive of finite-time attracting and repelling material surfaces and serve as finite time analogues of hyperbolic invariant manifolds, which have been classically used to study transport in autonomous dynamical systems. Given a vector field describing a nonautonomous dynamical system, the FTLE is a scalar field whose ridges represent pseudo-barriers across which transport is greatly hindered, a statement made formal by Shadden at al. [23]. Thus the FTLE field can be used to segment space into regions of related dynamical activity. This means that two particles starting in the same FLTE region will tend to flow together in time as the dynamical system evolves, whereas two particles straddling a ridge in the FLTE field, corresponding to a LCS instability, will tend to diverge exponentially in time. The flux of particles across an LCS approaches zero as the integration time for computation of the FTLE becomes larger [23]. These analytical tools allow one to quantify mixing in order to understand the dynamic mechanisms behind it.

Dynamical systems analysis, and more specifically LCS analysis, has been utilized in fluid dynamics to identify coherent structures and investigate mixing dynamics in a range of flows [20, 23-28]. Salman et al. [27] not only used the FTLE fields to identify the coherent structures in the flow field, but also to identify regions of entrainment caused by the structures. Haller and Yuan [20] applied dynamical systems analysis simulated two-dimensional turbulence to show that the material lines defined by the FTLE fields were responsible for stretching and folding motions in the mixing of passive scalars.

The application of dynamical system analysis to experimental data is less common due to the high spatial and temporal data requirements needed to perform the

needed integration (e.g. [26, 29-31]). Santitissadeekorn et al. [29] used the experimental data from Bohl [13] to identify the Lagrangian Coherent Structures (LCS) in the flow field. While this flow field is relatively "simple" compared to some flows for which dynamical systems analysis has been applied, the analysis was found to give insight into the physics of the flow field by identifying barriers to fluid transport in the experimental configuration.

I.3 Study Goals

The current work was initiated in support of the development of computational tools for the modeling of low Reynolds number mixing devices. The goals of the current work were to: 1) map out flow properties (e.g. the velocity, vorticity) in a simplified batch mixer for a variety of geometric and dynamic conditions, 2) utilize the experimental velocity data to determine the mixing potential of the flow fields, and 3) apply dynamical systems tools to explain the underlying physics of the mixing process. The current work expands on the work of Bohl [13] and Santitissadeekorn et al. [28] by examining the effect of blade position on the flow structure with respect to the tank wall and by quantifying the mixing for these geometries using the experimental velocity fields.

II. Methods

The experimental apparatus was a clear acrylic cylindrical container with an inside radius of r_w=6.93 cm and a clear flat bottom, Figure 1. Fluid motion was driven by a thin rectangular stainless steel blade rotated about its long axis by a variable speed DC motor. The blade was r_b = 2.99 cm (0.43r_w) wide and t_b=0.14 cm (0.02r_w) thick. The

rotational axis of the blade could be positioned at discreet offsets from the center of the tank of r_{off}= 0.0, 1.27, 2.54, 3.18, 3.81 cm (0.0r_w, 0.18r_w, 0.37r_w, 0.49r_w, 0.55r_w). The geometry was chosen as a simplified model of a batch mixer to provide simple, well defined boundary conditions for CFD model validation and verification and was the same as that studied by Bohl [13].

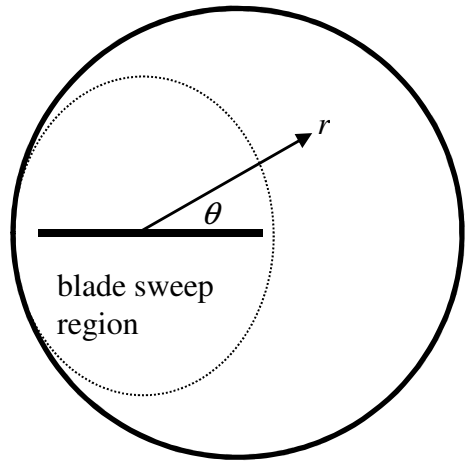

Figure 1: Schematic of experimental apparatus.

Three fluids, corn syrup, pure glycerin and a mixture of 85% glycerin and 15% water (i.e. "85/15") were used as the working fluids. The Reynolds number was defined as Re = $2\pi f r_w^2/\nu$ where f is the rotational frequency of the mixing blade. The three fluids produced Reynolds number of Re=0.02, 8 and 108. The Reynolds numbers chosen in this study bracket a change in the flow structure previously described [12, 13].

The origin of the coordinate system was located at the center of rotation of the blade, Figure 1, for all cases. When the blade was offset from the center of the tank this effectively moved the wall with respect to the blades so that the center of rotation was common for all offset cases. For descriptive purposes the blade sweep region was defined by the region of the flow swept by the mixing blades during rotation, as shown schematically in Figure 1.

The 2-D velocity in the fluid in the r-θ plane, at the mid-height of the fluid column, was measured using Particle Image Velocimetry (PIV). The fluids were seeded

with 10 μm silver coated glass spheres (S.G.~1.3) which showed no tendency to settle or float in the fluids used. Light was provided by a 4 Watt CW Spectra Physics Argon Ion laser pulsed using a NM Laser Products fast mechanical shutter. This shutter had a minimum closed-open-closed cycle time of 1 msec which was short enough that the imaged particles did not experience blurring during the exposure time. Images were captured using a Cooke Corporation 8-bit Sensicam-QE CCD camera (1376 x 1040).

The displacement of groups of particles was determined using a direct correlation technique [32]. Each Field-of-View (FOV) was approximately 8.7 cm x 12 cm in size (0.0087 cm/pixel) and covered nominally ¼ of the r-θ plane in the tank. The delay time between the images in each pair was set 10 msec to give maximum displacements of nominally 10 pixels. The source windows used in the correlation technique were 45 x 45 pixels (0.39 x 0.39 cm) with a 50% overlap.

The flow field under investigation was periodic in nature which allowed the data to be phase averaged with respect to the motion of the blade with a blade rotation broken into 128 bins. Phase averaged data from multiple experiments and multiple FOV's were combined to form a single data set. For all cases 788 images were acquired for each FOV. This resulted in approximately 12 measurements to be averaged for each phase bin. Investigation of the data showed that these results were repeatable to better than the experimental error at 9 measurements per bin. No-slip velocity boundary conditions were added during post processing.

The correlation technique used to process the data in this work is well documented [32] and has a 95% uncertainly level of 0.1 pixel. This corresponded to an uncertainty in the instantaneous velocity measurements of 0.08 cm/s. Phase averaging

and the combining of multiple data sets allowed multiple individual measurements to be averaged for a single measurement location. This reduced the estimated error in the presented data by a factor of 2 to 0.04 cm/s. Local vorticity was calculated using a second order finite difference method using the spatially nearest velocity measurements. Vorticity error was estimated to be 0.16 1/s [33].

Data sets for the offset cases were constructed by phase averaging data from 4 different FOV's, which, when combined covered the entire r-θ plane. Data for the centered blade cases were taken for a single FOV that covered the ¼ of the r-θ. A map of the entire container area was created by phase averaging the single perspective view taken, then rotating and combining those data to cover the entire area of the tank. It was found that long term integration flow field, required for mixing estimates, for the blade centered case could not be carried out accurately due to this method of data compilation. Therefore quantitative results of the mixing field could not be presented for the blade centered case.

All data presented in this work are from PIV measurements taken at the mid-height of the fluid column. Data not shown here indicated that the r-θ flow field was independent of the z-location over the middle half of the fluid column.

The LCS fields estimated here were computed numerically using the Runge-Kutta-45 integrator method. The base flow, together with the variational equations were (forward) coupled and therefore the integration had to be carried out simultaneously. A grid of initial conditions across the domain were simulated in order to estimate a view of the FTLE.

III. Results and Discussion

III.1 Phase Averaged Velocity and Vorticity

Past results [12, 13] show that at a vortex is formed at the tip of the mixing blade that rotates with the blade. A closed region of recirculation is formed between the tip and the cylinder wall if Re < 20 for the centered case. As the Re is increased the flow structure becomes more compact and asymmetric with a trailing region of vorticity extending downstream from the blade tip. It has also been shown that for Re = 0.02 and 8 the flow structure is quantitatively similar [13] therefore only the results for the Re=8 case will be presented in this work.

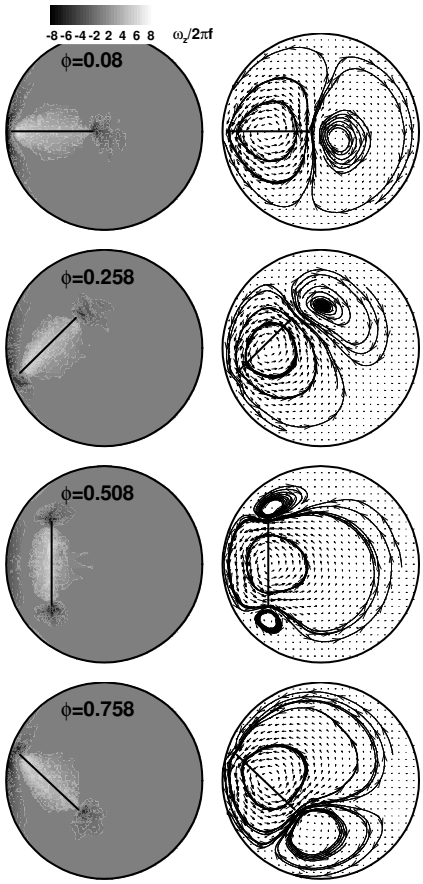

Figure 2: Vorticity and velocity vectors for r_{off}=0.55r_w. Re=8.

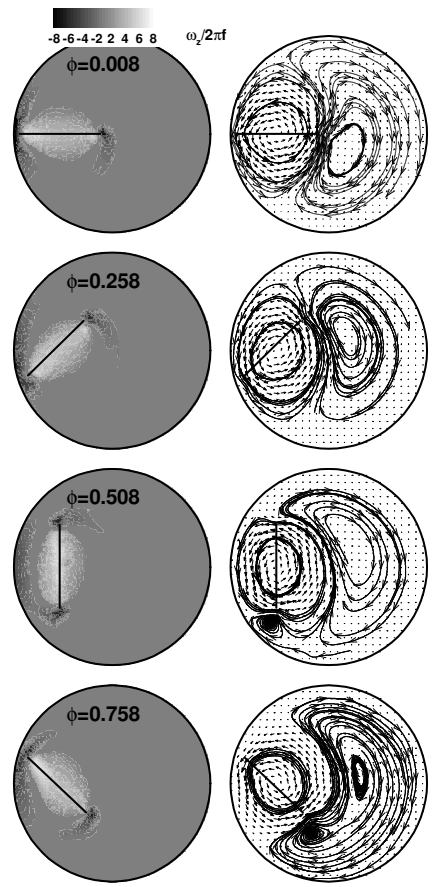

Figure 3: Vorticity and velocity vectors for r_{off}=0.55r_w. Re=108.

Figure 2 shows the Re=8 case for the largest offset (r_{off} = 0.55r_w). The vortex interacted with the container wall boundary layer as the blade tip approached the tank wall. This interaction strengthened both regions of vorticity with the peak value increasing from $\omega_z/2\pi f \approx -6$ to -10. The tip vortex and wall boundary layer then became indistinguishable from each. As the blade tip rotated away from the cylinder wall a region of vorticity separated from the wall to become the tip vortex that travelled through the remained of the rotation.

Figure 3 shows the Re=108 case. These data showed similar trends as was observed for the Re = 8 case. However, at this Reynolds number distinct differences in the flow patterns outside of the blade sweep region were observed. A large closed

recirculation region was observed outside of the blade sweep region. This region rotated slightly with the blade but did not follow the blade as it swept towards the wall remaining in a nominally fixed spatial region. The recirculation region created when the blade moved away from the cylinder wall followed the blade motion until it merged with the larger stationary region.

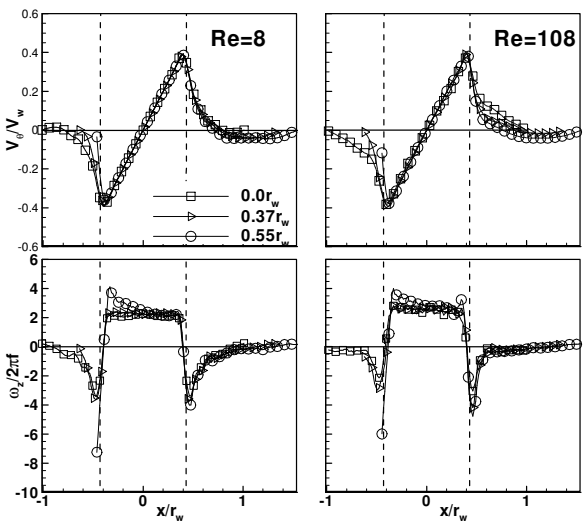

Figure 4: Velocity and vorticity profiles as a function of blade offset for Re=8, 108.

Line profiles of the circumferential velocity, V_θ, and the vorticity, ω_z, along the blade surface at ϕ=0.008 are shown in Figure 4. At Re=8 the closed recirculation regions were clearly evident by the change in sign of V_θ beyond the blade tip ($x > 0.6r_w$). The change in sign of V_θ occurred at nearly the same x-location indicating this phenomenon was relatively insensitive to the blade offset. Towards the wall ($x<-0.43r_w$) closed reverse flow was evident for all offset distances except at the largest offset (i.e. smallest gap) condition. The Re=108 data showed no evidence of reverse flow for the centered blade case. As the offset was increased the flow did reverse direction ($V_\theta < 0$) at this Reynolds number.

The peak vorticity profiles showed that the peak values of the tip vortical regions generated were only weakly dependent on the offset distance until the largest offset case, when the peak vorticity increased significantly. While the spatial resolution of the data

set was not fine enough to resolve the details of the boundary layer in the small gap region for this case, the trends clearly show an enhancement of the vorticity in the gap region.

III.2 FTLE Fields

The forward FTLE fields for the blade center case have shown that the flow is divided into regions separated by ridges (i.e. peaks in the FTLE field) near the blade tips [28]. These FTLE ridges acted as "barriers" inhibiting transport between regions in the flow [28], as proved by a flux integration [23]. It was therefore expected that the fluid contained within the blade sweep region should remain isolated from the fluid near the outer wall of the mixing tank. It was further inferred that the region where mixing should occur should exist primarily near the tip of the blade [28]. Data in the following sections also support these inferences from the FTLE fields. The results were found to be qualitatively similar for the Reynolds numbers studied with slight quantitative differences in the magnitudes of the FTLE fields, therefore only the FTLE fields from the Re=8 cases will be shown in the remainder of this work.

The FTLE fields as a function of phase for a blade offset of $0.55r_w$ are shown in Figure 5 for Re=8. The dominant feature in the FTLE field was a distinct ridge in the FTLE field above the upper surface of the blade for ϕ=0.008. This ridge had one end near the blade

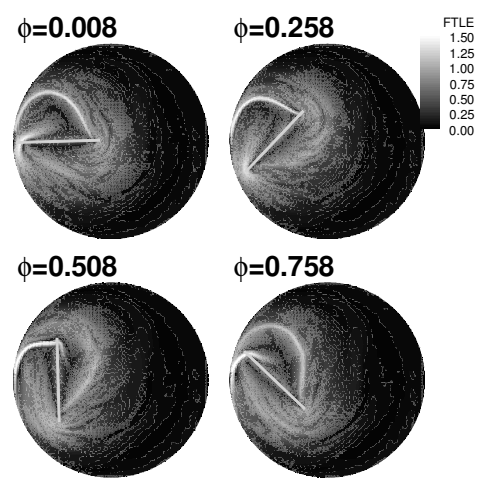

Figure 5: FTLE field for Re=8 at $0.55r_w$ blade offset.

tip with the second end near the wall location where the minimum distance between the blade tip and wall occurred. This ridge became shorter and the magnitude intensified as the blade tip approached the wall (see ϕ=0.258 to 0.508 to 0.758 to 0.008). As the blade tip swept away from the wall (ϕ=0.258) the ridge was least distinct.

Within the entire blade sweep region the FTLE field was relatively high in magnitude indicating higher local strain and mixing potential in this region. Outside of the blade sweep region the FTLE field was low which indicated lower local strain values indicative of low mixing potential outside of the blade sweep region. It was therefore expected that at this offset the mixing would be relatively high within the blade sweep region and low in the remainder of the tank.

The FTLE fields for different blade offset locations with ϕ=0.008 are shown in Figure 6. As the blade was positioned progressively more towards the center of the cylinder the FTLE ridge became less pronounced (i.e. the magnitude decreased and the width of the ridge increased).

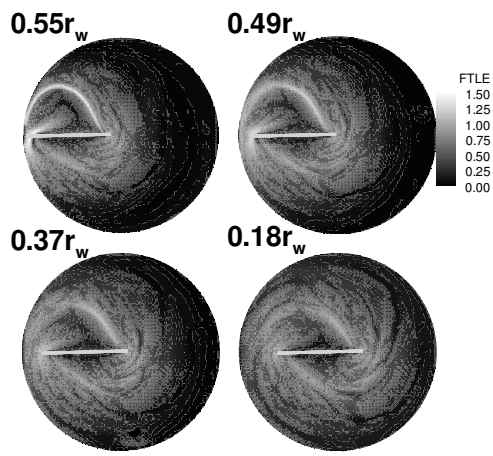

Figure 6: FTLE fields versus blade offset for Re=8 case.

The FTLE values in the region outside of the blade sweep area were observed to increase in magnitude as the blade offset was decreased. This indicated that the mixing level outside of the blade sweep area could be expected to be higher when the blade was centered in the container. In contrast, within the blade sweep area the FTLE values became progressively higher as the blade

was positioned closer to the cylinder wall indicating high mixing potential in this area as was positioned closer to the wall. The mean FTLE fields, Figure 7, support these results.

The previous figures show the FTLE results for relatively short integrations times of one half of a blade revolution. The integration time was extended and the results are shown in Figure 8 for the Re=8, r_{off}=0.55r_w case. A high intensity ridge was created for each blade half cycle. At 1 complete revolution two high intensity FTLE ridges were observed above the blade. The original FTLE ridge moved away from the blade sweep area and the intensity decreased however it was clearly recognizable. At 2.5 revolutions the ridges were still distinct, however by 5 revolutions the distinct structures in the FTLE field within the blade sweep region were no longer present.

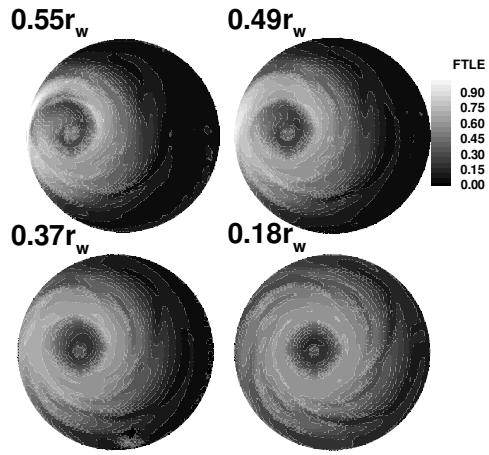

Figure 7: Mean FTLE fields for Re=8.

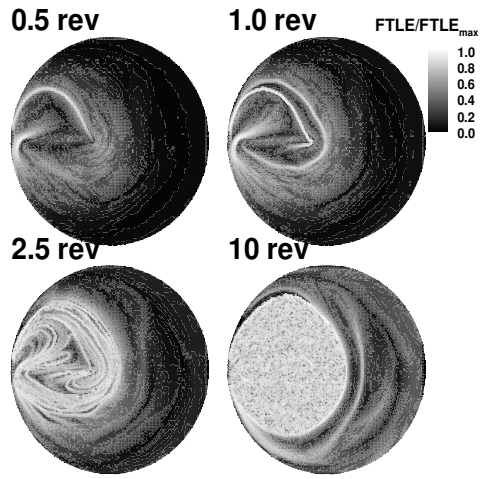

Figure 8: Normalized FTLE field as a function of integration time for Re=8 and r_{off}=0.55r_w.

The scaling in Figure 8 was normalized by the maximum in the FTLE field for the respective integration time. The maximum value in the FTLE field as a function of the number of rotations is shown in Figure 9. The data showed that the peak magnitude of the FTLE field decreased with number of rotations. This was interpreted by noting the theoretical ergodic limit. Long time integration of the

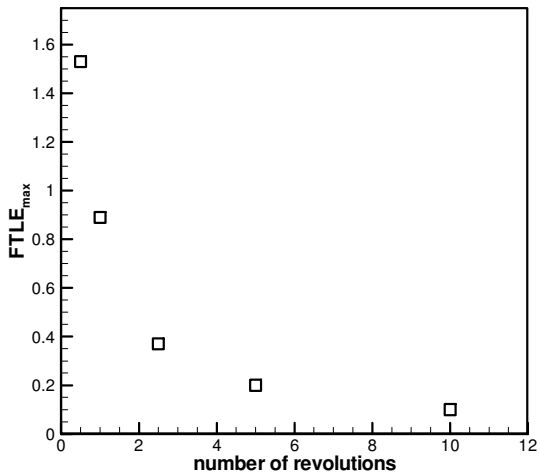

Figure 9: Maximum value in the FTLE field as a function of number of blade rotations. Re=8, r_{off}=0.55r_w.

FTLE field values will converge to the Lyapunov exponents independently of the initial condition for almost every initial condition in the ergodic region. Therefore, the apparent presence of a uniformly convergent FTLE region should be considered as indicative of an ergodic region. As such, in this region, the longtime behavior was of complete mixing. In contrast, the complement region did not become mixed even in the long term limit.

III.3 Mixing Fields

The experimentally derived velocity field was utilized to provide a quantitative estimate of mixing in the flow in the following manner. The flow field was "seeded" with two "species" of virtual zero mass point particles. The particle tracers, numbering 125,000 of each species, were initially uniformly distributed on the top and bottom half of the plane. These particles were convected by numeric integration (4th order Runge-Kutta) of the phase averaged velocity fields for up to 10 revolutions. The domain was divided into 24,000 cells and the number of black and white particles in each cell was determined to provide estimates on the mixing induced by the motion of the blade.

Figure 10 shows the fraction of particles in each cell for the Re=8 case with an offset of r_{off}= 0.18r_w. Stratifications were developed as the blade rotated through the fluid in the flow in the region near the blade tips. As the number of rotations increased these stratifications showed evidence of mixing at their interfaces though there remained

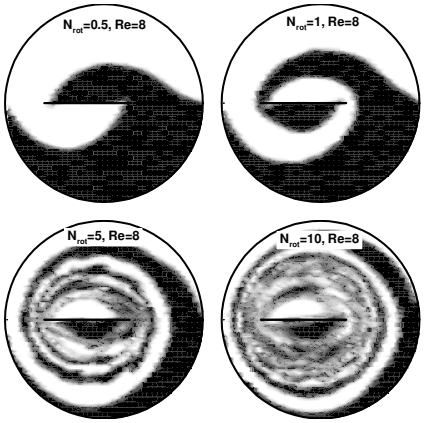

Figure 10: Plot of virtual particle locations as a function of blade rotations for r_{off}=0.17r_w. Species noted by black or white colors, greys indicates mixed regions.

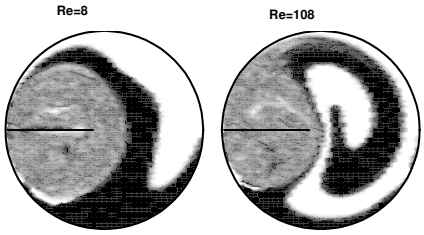

Figure 11: Plot of virtual particle locations for 10 blade rotations at r_{off}=0.55r_w. Species noted by black or white colors, greys indicates mixed regions.

distinct layers in the fluid. Distinct unmixed regions were observed on either side of the mixing blade and even after 10 rotations.

Particle distributions for the Re=8 and 108 cases with an offset of r_{off}=0.55r_w are shown in Figure 11. Striations were again formed for low number of revolutions (not shown); however, these striations were formed within the region swept by the blade. They quickly dispersed and after approximately 10 rotations the fluid within the blade sweep region appeared to be nearly homogenized with little evidence of single species regions.

Comparison of the particle maps, Figure 11, and the FTLE fields, Figure 8, for 10 rotations show them to be qualitatively similar. The location of the high FTLE region and the location of the mixed particles were spatially coincident in these two plots. Again, this long time behavior was suggestive of the ergodic region as noted . The ergodic region produces the same Lyapunov exponents for almost every initial condition (i.e. location), and as such, the presence of a region of same FTLE behavior independent of initial condition is suggestion of uniform mixing.

The data indicated that very little mixing occurred outside of the blade sweep region for the largest offset cases resulting in large single species regions. Both cases showed that particles starting in the upper half of the tank convected into the lower half nominally half way between the blade tip and the wall. Particles from the lower half of the tank were observed to convect into the upper half of the plane near the tip of the mixing blade.

At Re=108 the two single species regions began to turn back into each increasing the interfacial area. The location of this feature coincided with the nearly stationary location of the closed recirculation region. A region of well mixed fluid extended outside of the blade sweep region towards the top of the tank on the black/white interface. The particle patterns suggest that mixing outside of the blade sweep region occurred at the interface near the blade tips. In contrast, at Re=8 the black and white particles appeared to be entrained into the blade sweep area along the upper wall and were then mixed in the blade sweep region. The region of well mixed fluid appeared to expand laterally outward away from the blade tips into the tank region. These differences in the mixing fields are consistent with the differences in the flow fields already discussed.

A metric was derived to characterize the mixing potential of the flow using the particle locations. The mixing ratio, ξ, was defined for each cell as:

$$\xi = 2 * \frac{N_m}{N_{total}} \tag{1}$$

where N_m was the number of minor components in the cell and N_{total} was the total number of particles in the cell. The ratio N_m/N_{total} was multiplied by two so that a 50/50 concentration would be 100% mixed. The mixing ratios for all the cells in a specified

circular spatial region, defined by r_{mix}, were then averaged to determine the average mixing ratio, ξ_{avg} for the region.

The results of the average mixing ratio, ξ_{avg}, are shown in Figure 12 for the Re=8 case. Two mixing regions were considered in the analysis. First, the entire tank defined by r_{mix}/r_w=1(open symbols) and second only cells within the blade sweep region defined by r_{mix}/r_w=0.43 (closed symbols). The two different mixing regions were utilized to compare mixing within the entire tank to mixing in the proximity to the blade.

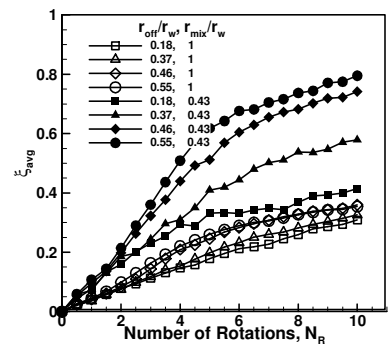

Figure 12: Plot of mixing ratios for Re=8 case versus the number of blade rotations.

Mixing in the entire tank was found to be lower than that observed in the blade sweep region for all offsets. The mixing ratio for the entire tank showed a high initial mixing rate until about 5 rotations after which the rate slowed. This initial higher mixing rate was due to the comparatively rapid mixing of the particles in or near the blade sweep region. The subsequently lower mixing rate was due to mixing of the particles outside of the blade sweep region caused by the slower secondary fluid motions.

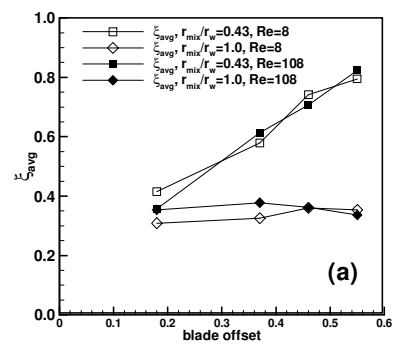

Figure 13: Comparison of mixing ratios after 10 blade rotations for Re=8 and 108.

Values of the mixing ratio after 10 rotations showed a mixed ratio of 30-35% for the entire tank with little dependence on the offset, Figure 13. Within the blade sweep region ξ_{avg}, was found to be significantly higher than was observed for the entire tank and

showed a nearly linear increase in the mixing level versus blade offset. It was clear from these data the interaction of the blade with the wall enhanced the mixing within the blade sweep region. After 10 rotations the mixing ratio was nearly 80% in the blade sweep region for the largest offset case. The data did not shown any clear Reynolds number dependence over the range investigated. Experiments were conducted in water (Re=5000) however the flow was found to be unsteady and could not be phased averaged successfully [13] and therefore FTLE and mixing analysis could not be performed on those data to extend the Reynolds number range.

It is instructive to note that while the mixing within the blade sweep region was significantly enhanced as the blade offset was increased, the mixing within the entire tank was nominally constant regardless of the blade offset. This result was due to the virtual lack of mixing outside of the blade sweep region for the larger offset cases. For the smaller offset cases the mixing in the blade sweep region was not as intense, however outside of that region the mixing occurred over a larger area. In a typical industrial batch mixer there would be multiple blades that rotate and orbit. The orbital motion is used to mix throughout the entire tank eliminating this low mixing region observed in the current experiments.

IV. Conclusions

In this work the flow in a cylindrical container, driven by the rotation of flat plates, was investigated using Particle Image Velocimetry. Three different Newtonian fluids (corn syrup, glycerin, and an 85/15 water/glycerin mixture) were used to provide Reynolds numbers of 0.08, 8 and 108 based on the tank radius and the rotational frequency of the blade. The flow field was interrogated for different blade offset

conditions to determine the effect of blade offset. The experimentally derived velocity fields were used to determine the Lagrangian Coherent Structures (LCS) and to estimate the mixing potential of the flow.

The velocity and vorticity fields showed that vortices were formed at the tips of the mixing blade. The vortical structures orbited with the blade and interacted with the boundary layer on the tank walls when the blade was positioned close to the wall. For the highest offset condition a closed recirculation region was observed in the tank away from the region swept by the blade at all Reynolds numbers. At Re=0.02 and 8 this region orbited with the blade tips, while at Re=108 this region was confined to a small region in the tank.

The LCS fields showed ridges developed in proximity to the blade tips. These regions were stronger and more distinct for as the blade offset was increased. For the smaller offset cases the ridges in the LCS fields were roughly circular around the blades and acted as a barrier between the fluid in the blade sweep region and the outer fluid. For the larger offset cases the LCS ridges were asymmetric about the blade and changed as the blade rotated.

Zero mass virtual particles were used to quantify the mixing potential of the flow field. The particle trajectories were found for up to 10 blade rotations by numerical integration of the flow field. For the small offset cases the particles formed distinct bands near the tip of the blade while within the blade sweep region the particles were largely unmixed. The number of bands formed was equal to the number of rotations of the blade. Mixing was found to occur in the regions where the bands were formed and stretched. For larger offset cases the particles within the blade sweep region quickly mixed and

became relatively homogenized. Outside of the blade sweep region the particles remained largely unmixed. The differences in the flow structures between the Re=0.02, 8 and 108 cases resulted in differences in the mixing and entrainment patterns.

The results of the mixing study showed that the averaging mixing in the entire tank was largely independent of the blade offset. Within the region of the flow swept by the blade mixing was enhanced as the blade was positioned closer to the wall while the mixing in the remainder of the tank was minimal. In contrast for the more centered blade positions the mixing in the tank outside of the blade sweep region was enhanced. This resulted in the nearly independent level of mixing in the tank as a function of the blade offset. The mixing values were also found to be minimally dependent on the Reynolds number for the cases investigated.

V. Acknowledgments

The experiments presented in this paper were conducted at the Naval Surface Warfare Center Indian Head Division in Indian Head Maryland through the internal CORE research program.

References

[1] Connelly, R. K., and Valenti-Jordan, J., 2008, "Mixing analysis of a Newtonian fluid in a 3D planetary pin mixer," Chemical Engineering Research & Design, 86(12A), pp. 1434-1440.
[2] Jongen, T., 2000, "Characterization of batch mixers using numerical flow simulations," Aiche Journal, 46(11), pp. 2140-2150.
[3] Tanguy, P. A., Bertrand, F., Labrie, R., and BritoDeLaFuente, E., 1996, "Numerical modelling of the mixing of viscoplastic slurries in a twin-blade planetary mixer," Chemical Engineering Research & Design, 74(A4), pp. 499-504.
[4] Finn, M. D., Cox, S. M., and Byrne, H. M., 2003, "Topological chaos in inviscid and viscous mixers," Journal of Fluid Mechanics, 493, pp. 345-361.
[5] Connelly, R. K., and Kokini, J. L., 2007, "Examination of the mixing ability of single and twin screw mixers using 2D finite element method simulation with particle tracking," Journal of Food Engineering, 79(3), pp. 956-969.

[6] Connelly, R. K., and Kokini, J. L., 2006, "3D numerical simulation of the flow of viscous Newtonian and shear thinning fluids in a twin sigma blade mixer," Advances in Polymer Technology, 25(3), pp. 182-194.
[7] Connelly, R. K., and Kokini, J. L., 2003, "2-D numerical simulation of differential viscoelastic fluids in a single-screw continuous mixer: Application of viscoelastic finite element methods," Advances in Polymer Technology, 22(1), pp. 22-41.
[8] Lindenberg, C., and Mazzotti, M., 2009, "Experimental characterization and multi-scale modeling of mixing in static mixers. Part 2. Effect of viscosity and scale-up," Chemical Engineering Science, 64(20), pp. 4286-4294.
[9] Lindenberg, C., Scholl, J., Vicum, L., Mazzotti, M., and Brozio, J., 2008, "Experimental characterization and multi-scale modeling of mixing in static mixers," Chemical Engineering Science, 63(16), pp. 4135-4149.
[10] Zhou, G., Tanguy, P. A., and Dubois, C., 2000, "Power consumption in a double planetary mixer with non-Newtonian and viscoelastic materials," Chemical Engineering Research & Design, 78(A3), pp. 445-453.
[11] Clifford, M. J., Cox, S. M., and Finn, M. D., 2004, "Reynolds number effects in a simple planetary mixer," Chemical Engineering Science, 59(16), pp. 3371-3379.
[12] Youcefi, A., AnneArchard, D., Boisson, H. C., and Sengelin, M., 1997, "On the influence of liquid elasticity on mixing in a vessel agitated by a two-bladed impeller," Journal of Fluids Engineering-Transactions of the Asme, 119(3), pp. 616-622.
[13] Bohl, D., 2007, "Experimental Investigation of the Fluid Motion in a Cylinder Driven by a Flat Plate Impeller," Journal of Fluids Engineering, 129(1), pp. 137-146.
[14] Jaffer, S. A., Bravo, V. L., Wood, P. E., Hrymak, A. N., and Wright, J. D., 2000, "Experimental validation of numerical simulations of the kneading disc section in a twin screw extruder," Polymer Engineering and Science, 40(4), pp. 892-901.
[15] Bakalis, S., and Karwe, M. V., 2002, "Velocity distributions and volume flow rates in the nip and translational regions of a co-rotating, self-wiping, twin-screw extruder," Journal of Food Engineering, 51(4), pp. 273-282.
[16] Yoon, H. S., Hill, D. F., Balachandar, S., Adrian, R. J., and Ha, M. Y., 2005, "Reynolds number scaling of flow in a Rushton turbine stirred tank. Part I - Mean flow, circular jet and tip vortex scaling," Chemical Engineering Science, 60(12), pp. 3169-3183.
[17] Utomo, A. T., Baker, M., and Pacek, A. W., 2008, "Flow pattern, periodicity and energy dissipation in a batch rotor-stator mixer," Chemical Engineering Research & Design, 86(12A), pp. 1397-1409.
[18] Haller, G., 2002, "Lagrangian coherent structures from approximate velocity data," Physics of Fluids, 14(6), pp. 1851-1861.
[19] Haller, G., and Poje, A. C., 1998, "Finite time transport in aperiodic flows," Physica D-Nonlinear Phenomena, 119(3-4), pp. 352-380.
[20] Haller, G., and Yuan, G., 2000, "Lagrangian coherent structures and mixing in two-dimensional turbulence," Physica D-Nonlinear Phenomena, 147(3-4), pp. 352-370.
[21] Haller, G., 2000, "Finding finite-time invariant manifolds in two-dimensional velocity fields," Chaos, 10(1), pp. 99-108.
[22] Haller, G., 2001, "Distinguished material surfaces and coherent structures in three-dimensional fluid flows," Physica D, 149(4), pp. 248-277.

[23] Shadden, S. C., Lekien, F., and Marsden, J. E., 2005, "Definition and properties of Lagrangian coherent structures from finite-time Lyapunov exponents in two-dimensional aperiodic flows," Physica D-Nonlinear Phenomena, 212(3-4), pp. 271-304.
[24] Wilson, M. M., Peng, J. F., Dabiri, J. O., and Eldredge, J. D., 2009, "Lagrangian coherent structures in low Reynolds number swimming," Journal of Physics-Condensed Matter, 21(20), pp. -.
[25] Beron-Vera, F. J., Olascoaga, M. J., and Goni, G. J., 2008, "Oceanic mesoscale eddies as revealed by Lagrangian coherent structures," Geophysical Research Letters, 35(12), pp. -.
[26] Vetel, J., Garon, A., and Pelletier, D., 2009, "Lagrangian coherent structures in the human carotid artery bifurcation," Experiments in Fluids, 46(6), pp. 1067-1079.
[27] Salman, H., Hesthaven, J. S., Warburton, T., and Haller, G., 2007, "Predicting transport by Lagrangian coherent structures with a high-order method," Theoretical and Computational Fluid Dynamics, 21(1), pp. 39-58.
[28] Santitissadeekorn, N., Bohl, D., and Bollt, E., 2009, "Analysis and modeling of an experimental device by finite-time lyapunov exponent method," Journal of Bifurcation and Chaos, 19(3), pp. 993-1006.
[29] Santitissadeekorn, N., Bohl, D., and Bollt, E. M., 2009, "Analysis and Modeling of an Experimental Device by Finite-Time Lyapunov Exponent Method," International Journal of Bifurcation and Chaos, 19(3), pp. 993-1006.
[30] Pan, C., Wang, J. J., and Zhang, C., 2009, "Identification of Lagrangian coherent structures in the turbulent boundary layer," Sci China Ser G, 52(2), pp. 248-257.
[31] Franco, E., Pekarek, D. N., Peng, J. F., and Dabiri, J. O., 2007, "Geometry of unsteady fluid transport during fluid-structure interactions," Journal of Fluid Mechanics, 589, pp. 125-145.
[32] Gendrich, C. P., and Koochesfahani, M. M., 1996, "A spatial correlation technique for estimating velocity fields using molecular tagging velocimetry (MTV)," Experiments in Fluids, 22(1), pp. 67-77.
[33] Bohl, D., and Koochesfahani, M., 2009, "*MTV Measurements of the Vortical Field in the Wake of an Airfoil Oscillating at High Reduced Frequency*," Journal of Fluid Mechanics, 620, pp. 63-88.

Figure Captions

Figure 1: Schematic of experimental apparatus.
Figure 2: Vorticity and velocity vectors for $r_{off}=0.55r_w$. Re=8.
Figure 3: Vorticity and velocity vectors for $r_{off}=0.55r_w$. Re=108.
Figure 4: Velocity and vorticity profiles as a function of blade offset for Re=8, 108.
Figure 5: FTLE field for Re=8 at $0.55r_w$ blade offset.
Figure 6: FTLE fields versus blade offset for Re=8 case.
Figure 7: Mean FTLE fields for Re=8.
Figure 8: Normalized FTLE field as a function of integration time for Re=8 and $r_{off}=0.55r_w$.
Figure 9: Maximum value in the FTLE field as a function of number of blade rotations. Re=8, $r_{off}=0.55r_w$.
Figure 10: Plot of virtual particle locations as a function of blade rotations for $r_{off}=0.17r_w$. Species noted by black or white colors, greys indicates mixed regions.
Figure 11: Plot of virtual particle locations for 10 blade rotations at $r_{off}=0.55r_w$. Species noted by black or white colors, greys indicates mixed regions.
Figure 12: Plot of mixing ratios for Re=8 case versus the number of blade rotations.
Figure 13: Comparison of mixing ratios after 10 blade rotations for Re=8 and 108.